Process Intensification for Zinc Dithionite Synthesis: Transition from Batch to Continuous Mesofluidic Reactor

Jean-Luc HOXHA[1*], Mathurin GROGNA[2], Sébastien CALVO[1], Dominique TOYE[1]

1: Department of Chemical Engineering, Liège University, B-4000 Liège, Belgium;
2: SILOX s.a., Rue Joseph Wauters 144, B-4480 Engis, Belgium.

**Corresponding author: jlhoxha@uliege.be / jeanluchoxha@gmail.com*

Highlights

- Development of a continuous intensified mesofluidic pilot flow reactor with consumption of solid particles.
- Batch tests reproducing industrial reactor performances.
- Continuous reactor modeling and parametric optimization of the zinc dithionite reaction kinetics.

Keywords
Process Intensification; mesoreactor; multiphase; experimental kinetics and continuous flow tubular reactor

Abbreviations
ID: Inside diameter
IR: infrared
OD: Outside diameter
PIV: Particle image velocimetry
Re: Reynolds number
RMSE: root mean square error
RMSECV: root mean square error of cross-validation
St: Stokes number
ZnHy: zinc hydrosulfite/zinc dithionite
ZnSu: zinc sulfite
ZnTi: zinc thiosulfate

Abstract

The synthesis of zinc dithionite was first performed in a batch reactor designed to mimic the industrial conditions. Experimental results demonstrated that increasing temperature negatively impacts dithionite selectivity, while the initial zinc concentration plays a critical role. The batch productivity is limited by the rate of SO_2 feed, which itself constrained by the temperature rise during the reaction. Based on the observations, the two key reactions are identified, leading to the production of zinc hydrosulfite and zinc sulfite, respectively:

1. $Zn_{(s)} + 2\ H_2SO_{3\ (aq)} \rightarrow 2\ H_2O_{(l)} + ZnS_2O_{4\ (aq)}$
   Rate law: $r1_{ZnHy} = -k1 * S_{Zn\_adim} * C_{SO2}$ [mol/s.m^3]
2. $Zn_{(s)} + H_2SO_{3\ (aq)} \rightarrow H_{2\ (g)} + ZnSO_{3\ (aq)}$
   Rate law: $r2_{ZnSu} = -k2 * (S_{Zn\_adim})^0 * (C_{SO2})^{0.5}$ [mol/s.m^3]

Here S_{Zn_adim} represents the normalized zinc surface relative to its maximum value in the batch reactor, and C_{SO2} denotes the concentration of SO_2.

A pilot scale continuous flow mesofluidic reactor fed with liquid SO_2 and an aqueous slurry of zinc particles was designed and then operated for dithionite production. Finally, a numerical model of the continuous reactor was developed, allowing the determination of the reaction kinetic parameters through least-squares fitting between experimental and simulated results (product concentrations). The adjusted data were used to model the concentration and temperature profiles in the reactor.

1. Introduction

Sodium dithionite ($Na_2S_2O_4$), also known as sodium hydrosulfite, is a product mainly used as a reducing or bleaching agent in textile, pulp, and paper industries. One of the possible industrial processes for the production of $Na_2S_2O_4$, called the "zinc process", involves the attack, in aqueous solution, of zinc particles by gaseous SO_2 in an open batch stirred tank reactor as described in Equation 1.

$$Zn_{(s)} + 2\,SO_{2\,(g)} \rightarrow ZnS_2O_{4\,(aq)} \quad (1)$$

The outcome of Equation 1 yields zinc dithionite, also known as zinc hydrosulfite (ZnS_2O_4) and designated as ZnHy, is an intermediate in the production of sodium hydrosulfite from this so-called "zinc process". The reaction effectiveness is limited by side reactions. One of them leads to the decomposition of zinc hydrosulfite into zinc sulfite ($ZnSO_3$), denoted as ZnSu, and other components as zinc thiosulfate (ZnS_2O_3), which become predominant if temperature increases and over a certain threshold T_{ref} [1], typically ranging between 40 and 90°C in industrial settings.
The final product of the first batch is then poured into a second batch filled with sodium hydroxide (NaOH) producing the desired final product, sodium dithionite from Equation 2.

$$ZnS_2O_{4\,(aq)} + 2\,NaOH_{(aq)} \rightarrow Na_2S_2O_{4\,(aq)} + Zn(OH)_{2\,(s)} \quad (2)$$

One advantage of this industrial zinc process is that it also produces another valuable product, zinc hydroxide ($Zn(OH)_2$). This hydroxide is mainly used for vulcanization purpose in the rubber industry [2].

The drawback of the batch zinc process is related to the control of the reaction exothermicity. As the synthesis reaction of zinc hydrosulfite is exothermic ($\Delta H \sim -234$ kJ/mol) [3], [4], [5], regulating the temperature in the industrial batch reactor requires the SO_2 feed to be staggered over time. This enables the reactor's heat exchange system (double jacket + coil) to extract the heat released by the reaction and maintain the temperature inside the reactor at its optimum level, equal to T_{ref} to avoid byproducts. However, staggering the SO_2 feed significantly increases the duration of the ZnS_2O_4 synthesis operation to approximately one hour and therefore limiting the productivity of the overall $Na_2S_2O_4$ production process. Another constraint associated with this process pertains to the preferential formation of zinc sulfite ($ZnSO_3$) as the reaction progresses and the pH of the solution decreases under a critical minimum threshold, possibly ranging from 2 to 4. Industrial important outcomes are the process selectivity defined as the ratio between ZnHy mass concentration to the ZnSu mass concentration and total zinc conversion ratio.

This paper delves into the study of this batch process, specifically the production of ZnHy, and explores methods for its intensification by running it continuously through an intensified flow reactor. Indeed,

contrary to batch reactors, which often entail extended operation and maintenance periods as well as poor heat transfer, continuous flow reactors have demonstrated several notable advantages. These include elimination of downtime, precise control over critical process parameters and consistent product quality. An intensified mesoscale continuous reactor will have an important surface to volume ratio and will thus enhance heat transfer efficiency and will, from its smaller volume, improve overall process safety. The utilization of mesoscale continuous flow reactors in chemical processes offers a promising avenue for more efficient and reliable production methods [6], [7], [8], [9], [10].

The main challenges of this process intensification are linked to the coexistence of gaseous, liquid and solid phases, which must be distributed and circulated within the reactor, while controlling the residence time in order to optimize the yield and selectivity of the desired reaction, i.e. the production of zinc dithionite.
A review of the literature shows that, in the case of continuous processes involving solid particles, efforts at intensification come up against the difficulty of ensuring intimate mixing of the reactants and avoiding plugging of the installation [11], [12], [13].

To tackle these challenges, researchers have explored alternative strategies, including the utilization of multiphase systems, innovative reactor geometries like helical or spiral configurations [14] and the incorporation of ultrasonic vibrations as well as oscillatory flow reactors to enhance mixing and mitigate the risk of clogging [15], [16], [17], [18], [19]. Nevertheless, wherever possible, it is advisable to avoid adding these more complex systems to reduce product costs, simplify production, and minimize the axial dispersion caused by these systems. Moreover, Bianchi [20] suggests that a balance must be struck between achieving effective particle suspension and minimizing axial dispersion.

As zinc hydrosulfite is not a high-value product, a successful transition requires the selection of a simple and robust technology, such as a tubular reactor. Two design approaches are possible: (1) a trial-and-error method, attempting numerous experiments to reach a satisfactory result, or (2) a custom-designed reactor based on a theoretical model developed from industrial knowledge of the involved reactions and on the influence of their operating conditions. Unfortunately, there is a scarcity of data on these reactions (mechanisms, kinetics, etc.) due to the fact that, in the discontinuous batch process, everything is governed by SO_2 supply rate and there are only few studies providing fundamental data.

In this case, a hybrid (iterative) approach was chosen, combining elements from both strategies. It consists of two steps:
First, the determination of the reactions and phenomena involved and the identification of potentially limiting steps from a literature review and from batch tests that mimic the industrial process. The latter enables the collection of data related to the reaction (composition, temperature and more).
Secondly, the collection and analysis of reliable experimental data on apparent kinetics. Lab batch tests provided access to the product distribution for different zinc conversion rates but were inconclusive regarding kinetics because, as said above, everything is controlled by the SO_2 injection rate. All other steps appear to be instantaneous. Thus, based on the partial available data (temperature range, reactant ratios), a mini-reactor in which operating conditions are perfectly controlled (heat transfer, residence time) was assembled to collect data giving access to the apparent reaction kinetics. This, in turn, will be used to design and optimize a mesofluidic-reactor.

This method allows for the practical flexibility of trial-and-error experimentation while leveraging theoretical insights to optimize reactor performance and minimize inefficiencies.

1.1. Reaction scheme

A proposal for the reaction scheme considered in this work with its kinetics model is presented below. The first and main redox reaction considered is the following, producing zinc dithionite:

$$Zn \rightarrow Zn^{2+} + 2\,e^-$$
$$2\,H_2SO_3 + 2\,e^- \rightarrow S_2O_4^{2-} + 2\,H_2O$$

$$\boldsymbol{Zn_{(s)} + 2\,H_2SO_{3\,(aq)} \rightarrow 2\,H_2O_{(l)} + ZnS_2O_{4\,(aq)}} \quad (3)$$

A publication by Sastri et al. [21], which explored a three-phase fluidization reactor, introduced this equation. Sastri and Epstein indeed worked on a fluidized bed with solid zinc, liquid water and pure gaseous SO_2 and thus had a high gas to liquid ratio. They reference Toor and Chiang's paper [22] on the absorption of sulfur dioxide in water showing that the dissolution of sulfur dioxide gas in water is directly followed by hydration and hydrolysis reactions which are in dynamic equilibrium. The available data on the absorption of sulfur dioxide in pure water show that the hydration and hydrolysis reactions occur in the fast regime. Eigen et al [23] determined the hydration reaction time to be equal to $0.3*10^{-6}$ seconds.
They estimated that the entire hydration and hydrolysis reactions are completed within 0.003 seconds and they concluded that the equilibrium prevails at each and every point and that kinetics become irrelevant when the chemical reactions are fast enough, as is observed in the absorption of SO_2 in water. Szabo and Káldi [24] also studied this reaction with gaseous SO_2. They presented two articles about SO_2 equilibrium from Lynn [25] and from Nijsing [26] that demonstrated that the equilibrium state among the forms is instantaneous.
Therefore, the reaction of SO_2 with water to form H_2SO_3 can be considered instantaneous, allowing the assumption that all introduced SO_2 is immediately converted into H_2SO_3.

Sastri and Epstein [27] and Sastri et al. [21] established that the zinc/sulfurous acid reaction for producing zinc dithionite can be considered first order with respect to acid strength. In the present study, a first-order dependency on sulfurous acid is similarly assumed. However, those earlier investigations did not account for the effect of the metal surface area. Here, the analysis is extended by considering a first-order dependance on the zinc particle surface area. This approach is consistent with findings from analogous systems; for example, studies on zinc dissolution in aqueous nitric acid have reported first-order kinetics with respect to both the zinc surface area and the concentration of HNO_2 [28].

Considering the production of zinc sulfite (ZnSu), a second redox reaction (eq. 4) is proposed.

$$Zn \rightarrow Zn^{2+} + 2\,e^-$$
$$H_2SO_3 + 2\,e^- \rightarrow H_2 + SO_3^{2-}$$

$$\boldsymbol{Zn_{(s)} + H_2SO_{3\,(aq)} \rightarrow H_{2\,(g)} + ZnSO_{3\,(aq)}} \quad (4)$$

The selection of this reaction is based on the fact that, in the batch reactor, a release of gaseous H_2 is observed, while no zinc thiosulfate (ZnTi) is detected in the products. So, even if suggested by several authors [21], [29], [30], [31], zinc sulfite may not come from the decomposition of zinc dithionite, because this reaction would lead to the production of zinc thiosulfate (ZnS_2O_3) which is not observed and cannot explain the presence of gaseous H_2.

Moreover, reaction (4) could explain the selectivity decrease at low pH. Indeed, Thomas et al. [32] reported that zinc corrosion in solutions depends on the range of pH: for pH higher than 4, zinc is passivated leading to negligible corrosion, while for pH between 3 and 1, zinc corrosion rate is related to the hydrogen production rate. So, reaction (4), which produces hydrogen, could explain why more ZnSu is produced at low pH, leading to a decrease in dithionite selectivity.

2. Material and Methods

2.1. Reagents

The experiments performed as part of the present research involved the following set of reagents:
- Liquid or gaseous sulfur dioxide (SO_2), purity $SO_2 \geq 99{,}98\%$
- Tap water at room temperature (20°C),
- Zinc dust
    - Gross-grade, particle size (Volumetric mean diameter = 24.15 µm), minimum $98\%_{w/w}$ metallic zinc
    - Ultra-fine grade (particle diameter ranging from 3 to 5 µm), min $98\%_{w/w}$ metallic zinc, minimum $99.5\%_{w/w}$ total zinc

2.2. Experimental setup

Two distinct setups were used successively: a batch reactor, designed to mimic the industrial process, and a continuous meso-flow reactor for conducting continuous experiments. Both setups are described in the following section.

Lab scale batch reactor

The setup presented in Figure 1 is designed to mimic the industrial process. It allows continuous monitoring of temperature and composition.

The batch reactor is a 3L tank cooled by a double-walled envelope. A Heidolph RZP 2102 electronic stirrer with a speed range from 0 to 2000 rpm and four inclined stirring blades, each with a surface area of $2.5cm^2$, is employed for efficient mixing in the reactor.

The reactor is initially filled with a mixture of water and zinc particles. SO_2 is then supplied from a pressurized cylinder at 1.7 bar. The gaseous SO2 injection is regulated with a UCAR ball rotameter that has a flow rate range of 0 to 150 L/h facilitated by a cylinder pressure reducer with a manometer and SO_2 consumption is also monitored by weighing the bottle containing the SO_2. The injection point is near the reactor's stirrer to improve bubble dispersion.

The reactor is further equipped with a Knick model Portamess 911 pH-meter coupled with a Toledo Reacg pro-425 pH-meter probe. The cooling system utilizes a Brookfield TC-650 circulating cooling bath with a flow rate of 12 L/min.

Figure 1. Lab batch reactor.

Continuous mesofluidic pilot-scale reactor

To transition from the batch stirred-tank reactor to a continuous tubular reactor, the reactants have to be adjusted accordingly.

It is no longer possible to work with gaseous SO_2 in this setup. Indeed, in this configuration, in order to maintain reasonable volumetric flow rates in the reactor, and thus significant residence times, while keeping the SO_2/Zn ratio in stoichiometric quantities for the nominal reaction (eq. 1), it is necessary to work with pressurized liquid SO_2. Otherwise, gaseous SO_2 would take up a considerable volume compared to the injected liquid, drastically reducing the residence time in the reactor and limiting contact between the two phases.

The pressure must be high enough to ensure that the SO_2 remains in liquid form in the reactor. It is set at 13 atm, chosen as high as possible according to the properties of all the components used in the setup. At this pressure (13 atm), SO_2 remains liquid up to a temperature of 67°C.

The zinc particles used were also adapted compared with the industrial batch reactor. A finer powder (maximum 5 microns) is used to minimize sedimentation.

Figure 2 shows a comprehensive scheme of the continuous installation. The setup comprises a ¼-inch outer diameter stainless-steel reactor equipped with a double jacket for cooling. The length of the reactor can be adjusted from 0.5 to 3 meters to vary the residence time. The pressure within the reactor is maintained at 13 atm by a Zaiput back pressure regulator. The reactor is fed by a Flusys WADose HPLC pump, which pressurizes and introduces liquid SO_2 from a SO_2 cylinder dip tube, and a Netzsch Nemo pump, delivering a constant slurry flow from a stirred container. The maximum flow rates of the two pumps are 40 mL/min and 210 mL/min, respectively. With an inlet flow rate of 210 mL/min and considering the inner section of the 1/4-inch tubing, the residence time in the reactor varies from 2.5 to 8.4 seconds depending on the total reactor length, which ranges from 0.39 to 1.2 meters.

The two reactants are mixed in an insulated JLS helical static mixer before entering a 1/4-inch stainless steel tubing enveloped by a 1/2-inch co-current water-cooling tube, with temperature control provided by a VWR cryostat bath with a maximum flowrate of 3 kg/min.

Temperature monitoring at the reactor outlet is facilitated by an EasyLog K-type thermocouple data

logger. Electrostatic, check valves and relief valves ensure process safety. Continuous analysis of samples at the reactor outlet is performed using a Thermo Scientific Nicolet Summit X IR spectrometer with a liquid flow cell. Additionally, samples can be taken for further analysis if needed. After analysis, the samples, along with the reactor output, are directed to a 25%$_m$ NaOH tank for SO_2 capture and product stabilization.

All junction tubes are made of transparent PTFA allowing visualization of the reacting fluid upstream and downstream of the reactor.

Temperature measurements are taken at location 1, and samples sent to the spectrometer are extracted at location 2 in Figure 2. This setup is mounted in a ventilated enclosure equipped with SO_2 detectors.

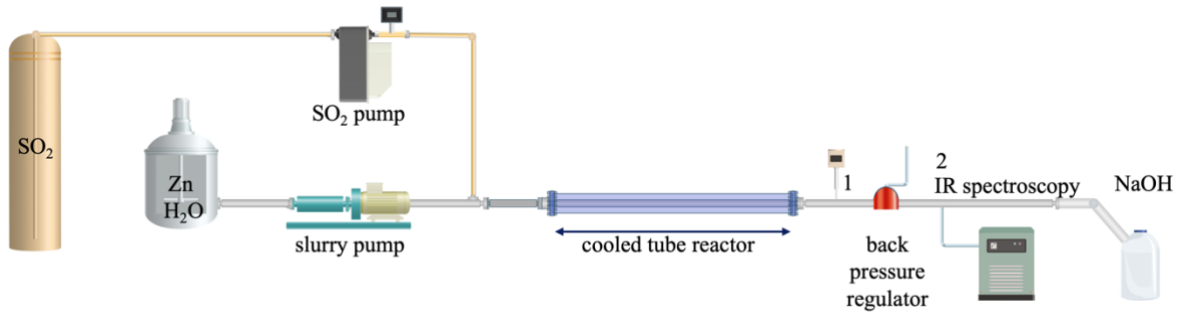

Figure 2. Simplified diagram of the mesofluidic pilot scale reactor.

The system operates as follows. The operation starts with the initiation of the pumps using water. After achieving a stable temperature in both the cooling system and the reactor, a transition from water to reagents, namely the slurry and SO_2, is facilitated by a valve system.

Following this stage, the reactor undergoes a transitional phase, and the progression from this state to a steady state is guided by monitoring the outlet temperature and ensuring the stability of spectrometer measurements. A consistent and stable outlet temperature over time indicates effective heat transfer performance and precise reactor control. [33]
To conclude the reaction and the experiment, the pumps are switched back to water, effectively purging the installation of all residual SO_2 and zinc. Subsequently, the pumps can be safely shut down, marking the completion of the entire process.

Visualization setup

A visualization setup was used for the characterization of the solid suspension within the continuous reactor described here above.

This experimental setup consists of the above continuous pilot-scale reactor followed with a quartz glass tube of 32 cm, OD of 6.2 mm and ID of 4 mm, after the cooled reaction tube section. This section was mounted in front of a high-speed camera equipped with a microscopic lens (Fastcam mini AX100, Photron – 12x zoom lens with x2 F mount adapter, Navitar). Videos were recorded with a framerate of 4000 fps, a resolution of 1024 x 1024 pixels (1 pixel = 5.9 x 5.9 µm^2) and a shutter speed of 1.05 µs to determine the solid concentration and velocity profiles. In order to achieve sharp images and videos, a strong LED light (Highpower LED, CREE) with a maximum of 2,180 lumen at 1 A was installed behind the tubing. This LED light was controlled by a voltage controller with a constant current of 0.3 A and the LED was placed on a heat sink.

2.3. Characterization techniques

The composition of the reactional mixture can be measured either by iodometric titration [34], [35], [36] or by infrared spectroscopy.

The iodometric titration method is the method used for batch reactor experiments as it is the method used in the industrial process. It is a robust and inexpensive, but time-consuming method.

IR spectroscopy is employed in the continuous reactor. The IR spectrophotometer used in the present study is a Thermo Scientific Nicolet Summit X spectrometer with an ATR flow cell of 100 µL. This analytic technique is increasingly used with flow-cell facilities to carry out non-invasive measurements in real-time [37]. Its short response time and the possibility of on-line implementation makes it capable of characterizing the composition at the continuous reactor exit. This on-line analysis device can also be integrated into the process control loop, enabling real-time adjustment of feed rates, setpoint temperatures and other parameters to respond effectively to disturbances [37].
IR spectroscopy is documented for the analysis of sodium hydrosulfite [1], [38]usually not applied for zinc dithionite and zinc sulfite analysis. Therefore, the method had to be validated for the products of interest in this study (zinc hydrosulfite and sulfite). To this end, IR measurements were calibrated and validated through comparisons with iodometric titration results. The parameters for the IR spectra interpretation were fitted based on results from iodometric method using a partial least square regression method (PLS). This technology thus allows monitoring the formation of desired and undesired products [39]. Figures 3(a) and 3(b) compare the dithionite and sulfite concentrations measured by titration with concentrations calculated from IR spectra. Their concentrations have been normalized by the maximum measured concentration of each product.
The RMSECV (root mean square error of cross-validation) of the normalized values is 0.008 for dithionite and 0.053 for sulfite. Even if normalized errors are larger for sulfite, it is not the case for absolute errors as the error associated with sulfite is approximately 65% lower than that for dithionite as its concentration is smaller.

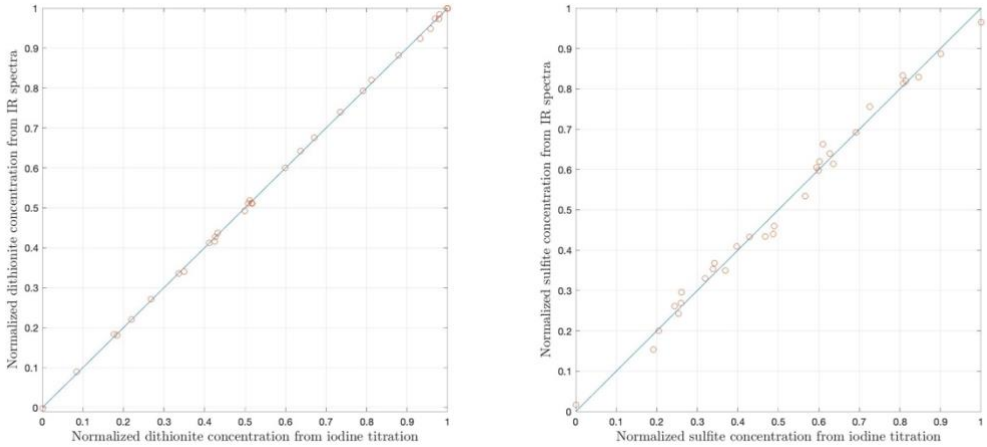

Figure 3: (a) Normalized comparison between dithionite concentrations from IR spectra and from iodine titration (b) Normalized comparison between sulfite concentrations from IR spectra and iodine titration.

2.4. Modeling and simulation

Zinc dithionite production in a continuous flow tubular reactor is a multiphase solid-consumption process that involves two phases: a liquid phase (water, SO_2, reaction products) and a solid phase (zinc particles). Modeling such a process requires accounting for all phenomena that occur simultaneously as heat transfer, reaction kinetics and fluid dynamics, as well as their coupling.

In a first step, the mathematical model developed is based on three main assumptions: (1) the liquid flow is considered to be ideal plug flow, (2) zinc particles are considered perfectly spherical and monodisperse in size (3) the solid zinc particles are considered to be perfectly suspended and their concentration assumed to be radially homogeneous, i.e. the slurry is considered homogeneous, with solid particles perfectly following the liquid flow. As a result, no population balance is considered as particles shrink uniformly as the reaction progresses and were already considered monodispersed in size at the reactor inlet.

The following equations must be solved to run the model:

Steady-state mole balances on a PFR:

$$\frac{dF_j}{dV} = r_j \tag{5}$$

Energy balance on the reactor:

$$\frac{dT}{dV} = \frac{r_i \Delta H_R - Ua(T - T_a)}{\sum(F_{A0}(C_{Pi} + \Delta C_{Pi} X))} \tag{6}$$

Energy balance on the cooling system:

$$\frac{dT}{dV} = \frac{Ua(T_a - T)}{m_c C_{P_c}} \tag{7}$$

The kinetics of the zinc dithionite and zinc sulfite production reactions are surface reactions.

The apparent reaction rates considered are respectively as follows:

r1 = -k1 *S_Zn_adim * C_SO2 [mol/s.L] where k1 = A1 * exp(-Ea1/(R*T)) (8)

r2 = -k2 *S_Zn_adim^0 * C_SO$^{0.5}$ [mol/s.L] where k2 = A2 * exp(-Ea2/(R*T)) (9)

where F_j is the molar flow rate of species j (mol/s),

V is the volume of reactor (dm^3),

r_j is the rate of generation of reaction i per unit volume ($mol/s.dm^3$),

T is the temperature (K),

r_i is the rate of generation of species j per unit volume ($mol/s.dm^3$),

ΔH_R is the standard enthalpy of reaction,

U is the overall heat transfer coefficient between the reacting flow and the coolant ($J/m^2.s.K$)

a is the area of heat exchange per unit volume of reactor (m^{-1}),

T_a is the temperature of the cooling system (K),

C_{Pi} is respectively the specific heat capacity of species i (J/mol.K),

X is the conversion of the key reactant,

E_{ai} is the activation energy (J/mol) of reaction i,

S_Zn_adim is the available zinc surface relative to its maximum value in the batch reactor,

R is the ideal gas constant.

To model the phenomena occurring in the reactor (flow, reactions, heat transfer), the MATLAB software with the Optimization toolbox was employed.
The reactor is modelled as a series of three plug flow reactors:
The first section is 25 cm long, beginning from the feed junction where the reactants come into contact in a static mixer before entering the second section. This section is insulated and considered adiabatic.
The second section is a stainless-steel double-jacketed reactor with a co-current cooling system, the length of which varies depending on the lab experiments (ranging from 39 to 120 cm).
The third and final section is also insulated and considered as adiabatic. It corresponds to the 25 cm tube between the temperature measurement location at the cooled reactor outlet and the sampling point for the IR spectrophotometer, where reactions are still ongoing.

Heat transfer coefficient
An effective value of the heat coefficient for the double-jacketed reactor (second section) has been determined experimentally under various conditions, including different water inlet temperatures, reactor lengths, and cooling or heating temperatures. The resulting value of U is 1035 J/(m^2.s.K). This value has been considered constant across the different operating conditions.

The non-isothermal reactor model is applied to simulate both concentration and temperature axial profiles. These profiles are computed for various operating conditions and different reactor lengths (section 2). For each case, the computed values at locations corresponding to the experimental measurements points in the setup are extracted to enable direct comparison with experimental data collected from the pilot reactor.

3. Results and discussion

3.1. Batch reactor results

The study of the phenomena occurring in the batch laboratory reactor, described in Section 2.2, is carried out by varying one parameter at a time. Precise measurements of various parameters (concentrations, temperatures, granulometry, agitation) are used to determine the limiting phenomena.

The figure below (Fig. 4) presents typical results from a lab batch reactor test. It shows the evolution of pH, temperature and selectivity as a function of the amount of cumulated SO_2 injected. As SO_2 inlet flowrate is not constant, the x-axis is therefore not linear with respect to time. For reasons of confidentiality, except for selectivity which is defined as the ratio between ZnHy mass concentration to the ZnSu mass concentration, the figure axis are normalized using the maximum measured value of each parameter. The experimental results (concentrations, temperature, and final selectivity) obtained from

the laboratory-scale batch reactor closely align with those observed in the industrial batch process. The relative variation in selectivity between the laboratory and industrial batches is approximately ±3, depending on the specific batch.

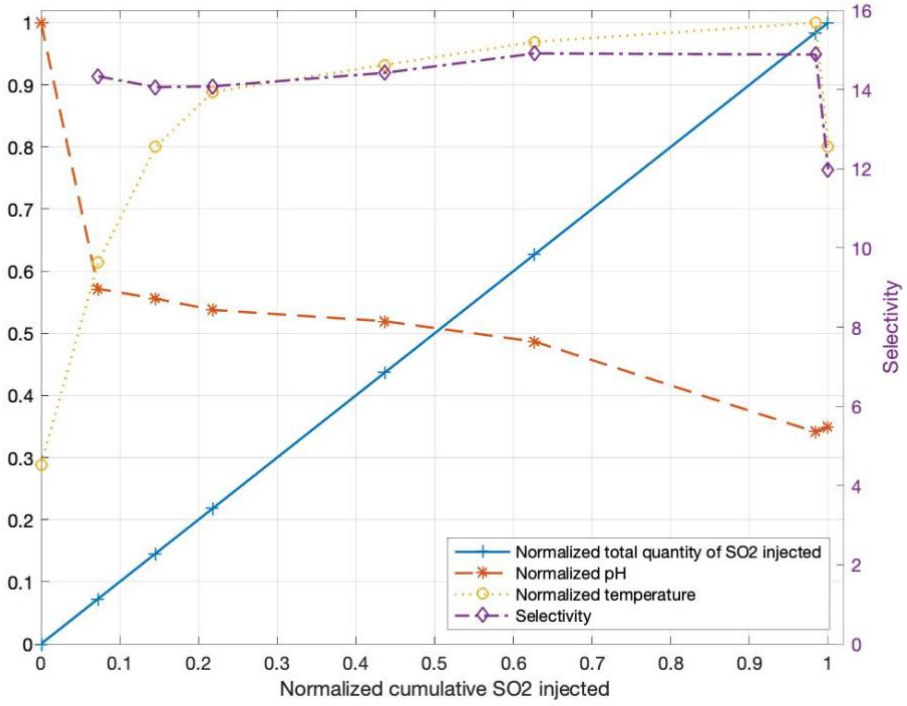

Figure 4: Normalized temperature, pH, cumulated injected SO_2 and mass selectivity during a lab batch reactor experiment.

Initially, the injection of SO_2 is rapid and due to the high exothermicity of the reaction, the reactor's temperature increases. This causes a decrease in the pH of the solution. Subsequently, the SO_2 flow rate is adjusted to maintain temperature as constant as possible, slightly below its peak value. In the corresponding figure, this maximum temperature is normalized to 1 and designated as the reference temperature T_{ref}, as introduced in the introduction. Throughout the test, the temperature remains almost constant (referred to as the plateau temperature), serving as a control variable. Meanwhile, pH decreases continuously and selectivity (zinc hydrosulfite/zinc sulfite) is maintained at a high level. It can be seen that selectivity decreases at the end of the reaction. Nevertheless, this selectivity drop occurs at low pH values within an acidic range (approximately 4 to 2) near the end of the batch operation in the industrial process. Even though detrimental for selectivity, the industrial batch process is not stopped before because it allows a higher zinc consumption. Furthermore, the presence of the by-product, zinc sulfite, is not so detrimental for the global process as it also leads to the second end-product, zinc hydroxide, in the further process steps. Zinc conversion remains thus high, with a minimum of 90%, depending on the quality of the zinc used.

Figure 5 presents the cumulated quantity of SO_2 converted into zinc hydrosulfite (yellow) and zinc sulfite (orange), respectively. The sum of these two quantities (purple) represents the total SO_2 that reacted as a function of the cumulated amount of SO_2 injected into the reactor during laboratory test.

This figure illustrates that during a batch reaction, even when SO_2 is injected at the maximum possible rate (at the beginning), it reacts completely with the zinc dust. This indicates that, under these conditions, the rate of reactant consumption is constrained by the SO_2 injection rate, which is itself limited by the temperature control. To test this hypothesis, the initial quantity of zinc was halved and then quartered while maintaining the same SO_2 flow rate. These experiments demonstrated that, even with reduced zinc quantities, the SO_2 injection rate always remains the limiting factor in the batch reactor.

Throughout the process, there is minimal loss of SO_2, meaning that virtually no non-reacted SO_2 escapes in the gas phase exiting the reactor. However, small losses are observed towards the end of the reaction when the available zinc becomes very low. The total unreacted SO_2 is evaluated to 5.7% of the total SO_2 injected. The cumulative SO_2 injected value is therefore close to the stoichiometric ratio relative to the total initial zinc.

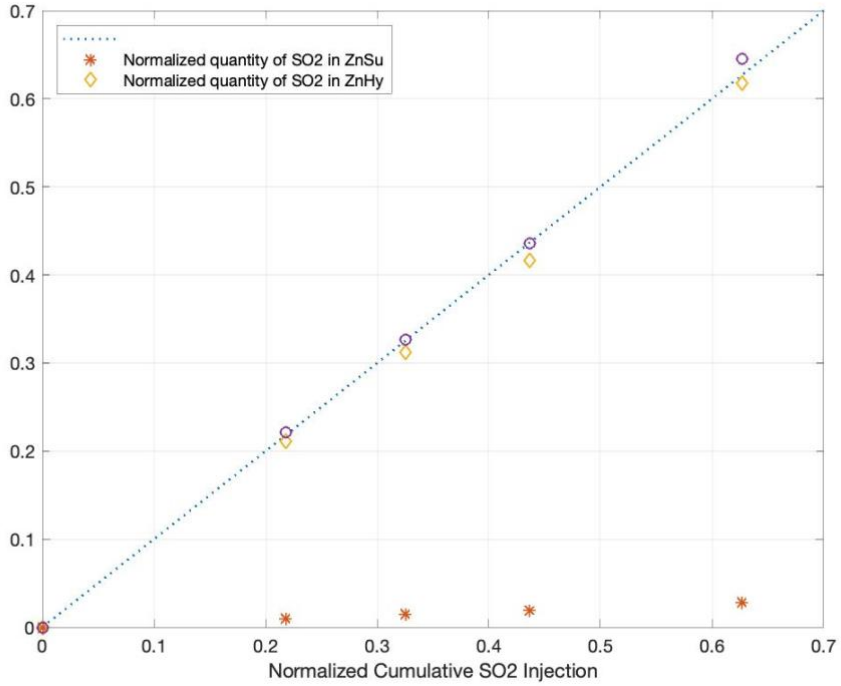

Figure 5: Evolution of SO_2 consumed as a function of cumulated injected SO_2 for a Zn concentration equivalent to the industrial reactor during a lab batch reactor experiment.

The experiments carried out show that under the current process conditions, the overall kinetics of the process is conditioned by the rate of the injection of SO_2, which is itself limited by the temperature control. It is therefore not possible to measure the intrinsic kinetics of the chemical reaction in this setup.

Temperature effect

Temperature has potentially different effects on reaction kinetics. Increasing temperature leads to higher reaction rates according to Arrhenius' law. Temperature can therefore influence the ratio of the desired product, zinc dithionite, to the secondary product, zinc sulfite, if reactions (eq. 3 and eq. 4) have different activation energies. Reactor temperature was maintained as constant as possible by varying cooling temperature.

The results obtained show that there is a correlation between the plateau temperature during the batch process and the final selectivity (ZnHy compared to ZnSu). Final ZnHy and ZnSu concentrations in Table 1 have been normalized relative to the average industrial final concentrations of each component

at the end of the process. As shown in this table, the higher the temperature, the lower the final selectivity and it shows that the production of ZnSu is significantly more impacted by the increase in temperature.

Table 1 : Correlation between reactor temperature and final selectivity for different experiments.

Normalized temperature [/]	Normalized ZnHy concentration [/]	Normalized ZnS concentration [/]	Final selectivity [/]
0.80	1.007	0.883	11
1	0.997	1.120	8.6

Effect of the initial zinc concentration

The effect of the initial zinc concentration in the slurry was also studied in order to detect a possible correlation between this initial zinc/water ratio and the selectivity at the end of the reaction. The SO_2 injection was stopped using the same criteria as in the industrial process, specifically based on the pH of the solution.

When different amounts of zinc are used for the same water volume in the batch reactor, the plateau temperature during the reaction is impacted: for smaller zinc concentrations, the heat released by reaction is also less important, so the cooling system can maintain a lower plateau temperature (as shown in Fig. 6).

As presented in Fig. 6, the results show that higher initial amounts of zinc lead to higher final selectivity values. Increasing the initial zinc concentration is advantageous for maintaining a higher final selectivity at the end of the reaction despite the higher temperature which could impact final selectivity negatively.

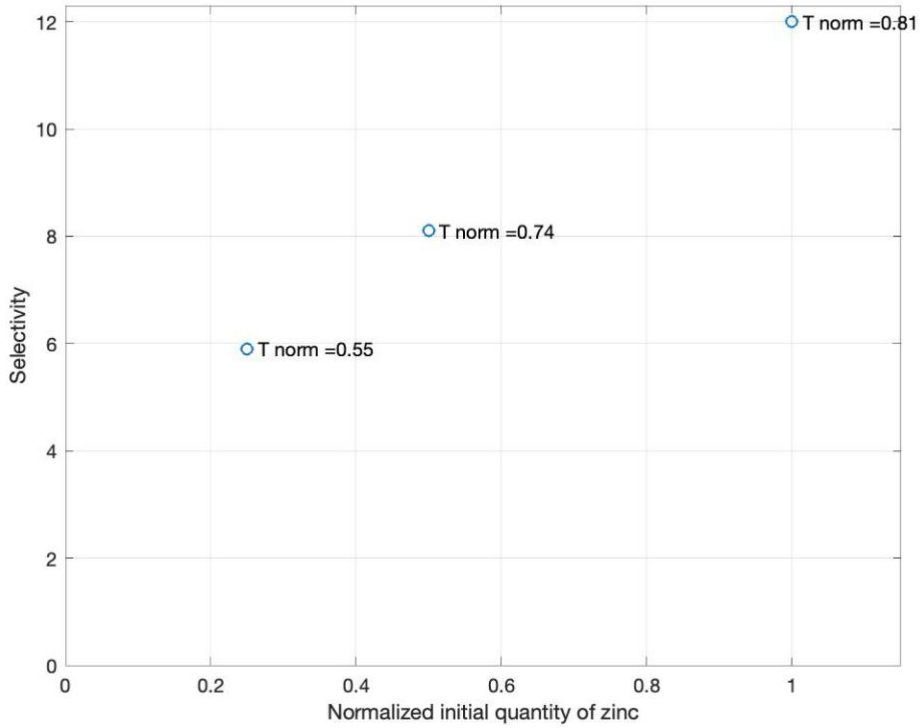

Figure 6: Final selectivity for different experiments as function of the initial zinc concentration.

In conclusion, zinc concentration is a critical parameter, the value of which must be optimized when operating the continuous reactor, since a higher zinc concentration achieves higher final selectivity values, but also increases the risk of the reactor becoming clogged with solid particles.

3.2. Mesofluidic reactor results

In a first step the multiphase flow in the reactor was characterized to test the validity of the model's hypothesis, i.e. liquid plug flow and uniformly suspended solid particles.

Liquid flow

In order to verify the first assumption of the model (plug flow reactor), the Reynolds number (Re) is calculated for the mean experimental flow to determine the flow regime of the fluid in the pipes. The obtained Reynolds number is approximately 1600. Given the low Reynolds number, the flow in the reactor is not turbulent, indicating that the theoretical Péclet (Pe) number does not support the assumption of plug flow [40].

Tracer tests using a NaCl solution were performed to characterize the system's flow behavior and residence time distribution. Due to the placement of the injection point located upstream of the slurry pump and two measurement point at the reactor inlet and outlet, the tracer curves were strongly influenced by the pump's large, well-mixed volume. This influence obscured the reactor's intrinsic dispersion characteristics, making it difficult to extract detailed distribution parameters necessary for validating the plug flow assumption or quantifying axial dispersion. Consequently, the only reliable parameter obtained from these tests was the mean residence time, which was found to correspond well with theoretical calculations based on the liquid flow rate and reactor volume.

Despite these findings, the plug flow assumption was initially adopted due to the significant simplification it brings to the modeling process (for later kinetics optimization). Therefore, an iterative approach was chosen, where the initial modeling step employs an ideal plug flow assumption. This approach allows for a more straightforward analysis while providing a basis for further refinement if necessary, depending on experimental outcomes and reactor optimization needs. This procedure is justified by the fact that it is known that, for moderate conversion values, axial dispersion has a limited impact on overall reactor performance.

Solid suspension

Given that a static mixer is placed at the reactor inlet, the solid particles are well distributed within the feed stream. To check if this good dispersion is maintained along the reactor length and that the solid particles perfectly follow the liquid flow, the Stokes number (St) was calculated. This non dimensional number serves as an indicator of the relationship between particle and flow characteristic times. It plays a pivotal role in assessing particle dynamics within a flowing fluid. The Stokes number calculated for particles with a size of 5 µm in a flow rate of 200 mL/min ranges between 10^{-3} to 10^{-4}, which is significantly smaller than the threshold value of 0.1. Particles should therefore follow the flow and there should be no sedimentation in the reactor, unless the possibility of particle agglomeration is considered. [41]

The visualization setup described in section 2.2 was used to characterize the distribution and the velocity of solid particles in the reactor. As shown in Figure 7, a homogenous and almost perfect suspension of

zinc is experimentally observed at the reactor outlet, when small zinc particles (3-5 microns) are used. Similar experiments using larger particles (like those employed in the batch reactor) demonstrate that it is essential to work with finer particles to avoid sedimentation.

As shown in Fig.7, the tests carried out reveal that a certain accumulation of solids appears in the lower part of the tubular reactor (due to the presence of agglomerates or of larger particles). This accumulation is confirmed as luminosity passing through the reactor decreases if zinc concentration increases.

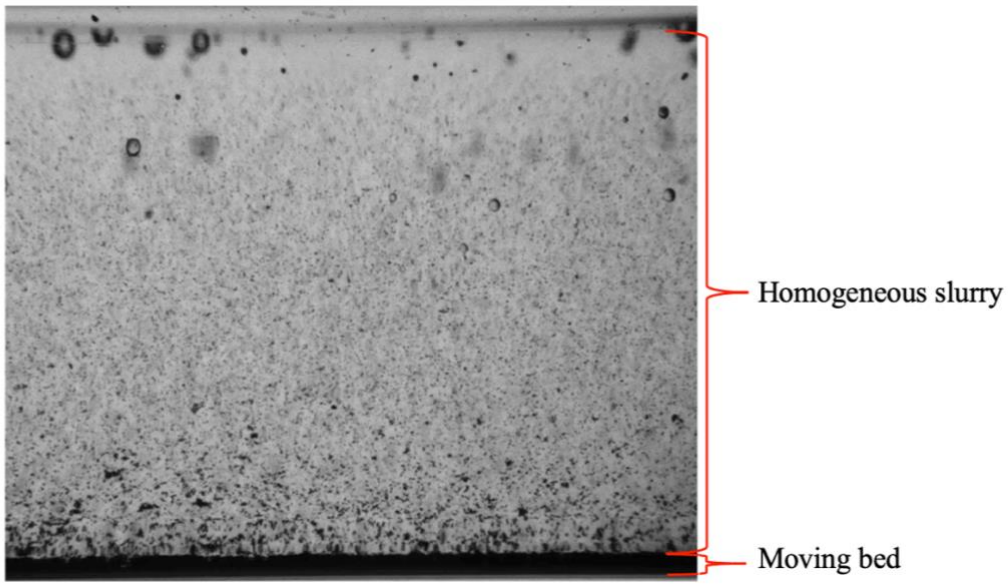

Figure 7. Image from the visualization setup of the 3-5 microns particles in the ¼ inch tube.

From the recorded images and videos, it appears that a thin moving bed forms at the bottom of the tubular reactor. The height of the moving bed is approximately $1/25^{th}$ of the tube diameter, corresponding to 1.3% of the total reactor volume, which is negligible. Moreover, there is no temporal accumulation of zinc at the bottom of the reactor. However, more advanced reactor designs should incorporate additional measures to improve suspension, such as the integration of static mixers.

Velocity profile

The visualization equipment was also used to measure velocities using image analysis tools, taking advantage of the high contrast between the dark particles and the illuminated background under blacklight. This contrast facilitated precise tracking of particle motion, enabling accurate velocity measurements. The average particle velocity and its radial profile, obtained from images analysis performed in PiVlab v3.01 for MATLAB, can be compared with the average liquid velocity and the theoretical laminar flow profile from Poiseuille equation. This theoretical laminar profile has been shifted upwards to account for the presence of the moving bed at the bottom of the tube, in which velocity cannot be measured accurately. The velocity profile of the solid phase closely approximates a parabolic shape and matches the same maximum velocity as the theoretical laminar velocity profile from Poiseuille equation (Fig. 8). This indicates that the particles move at the same speed as the liquid phase and thus that the solid particles efficiently follow the liquid flow. This observation aligns with the Stokes number value calculated in the previous section.

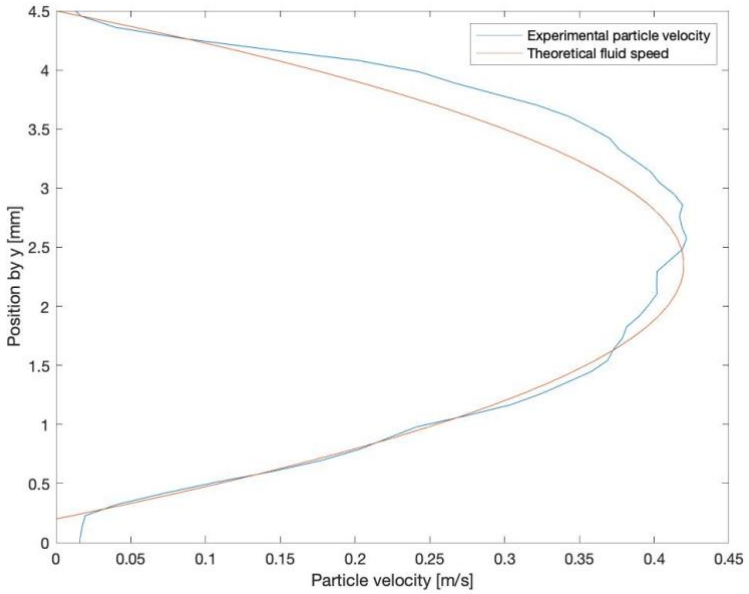

Figure 8. Experimental velocity of the particles and theorical laminar velocity as function of the height position in the tubular reactor.

Particle size distribution

A unique particle size is considered in the model due to their very narrow size distribution (3-5 microns) at the reactor inlet. The population balance is not addressed in this model because several key assumptions simplify the analysis. Specifically, it is assumed that the reactions are homogeneous on the zinc particles, which remain spherical as demonstrated by Sastri and Epstein [27], who showed that zinc dissolution occurs uniformly without pitting. Consequently, the number of particles remains constant while their radius and thus surface area decrease uniformly with residence time. Population balance considerations would typically be necessary if flow deviated from ideal plug flow, as this could lead to varying chemical compositions and reaction progress at different radial positions within the reactor, affecting particle size evolution due to differential residence times. Similarly, non-uniform particle distribution could introduce local variations in concentration, impacting reaction rates and particle size changes. However, under the current assumptions of uniform flow, homogeneous reaction conditions, and consistent particle distribution, these complexities are minimized, making a detailed population balance analysis unnecessary for this model.

Experimental results

The detailed description of the pilot continuous flow reactor used for zinc dithionite synthesis can be found in Section 2.2. Different tests were conducted under various experimental conditions. The length of the cooled system varied from 0.39 to 1.2 meters, the temperature of the cooling system ranged from 3 to 20°C, the slurry flow rate was kept constant at 210 mL/min, the volumetric percentage of zinc in the slurry was also varied (normalized values compared to the batch concentration), and the SO_2 flowrate was adjusted from 0 to 40 mL/min). For each test, concentrations and temperatures were measured once the reactor reached steady state.

It was observed that the volumetric percentage of zinc was a critical parameter for avoiding flow and pressure fluctuations that could lead to clogging and unsteady concentration values. Therefore, to

prevent any risk of installation clogging during experiments aimed at defining the kinetics model, the concentration of zinc in the slurry were intentionally reduced.

Table 2 summarizes the various input variables from the laboratory experiments and presents the resulting normalized values of outlet concentrations and temperatures for each case.

Table 2: Experiment input variables and outlet concentrations and temperatures.

Number	Cooled reactor length (m)	Normalized ratio H2O/Zn	Slurry flow (mL/min)	T cool (°C)	SO2 flow (mL/min)	T out (°C)	Normalized [ZnHy]	Normalized [ZnSu]	Selectivity
1	1.2	2.30	210	5	30	33.50	0.39	0.44	8.37
2					34	38.77	0.41	0.38	10.47
3					36	40.93	0.43	0.30	13.74
4				15	30	40.31	0.39	0.40	9.45
5					38	45.88	0.45	0.54	8.04
6				3	36	36.91	0.44	0.54	7.74
7					38	37.84	0.45	0.68	6.35
8					20	28.55	0.29	0.17	16.01
9		4.60		5	0	9.98	0.00	0.03	n/a
10					10	20.20	0.15	0.25	5.65
11					15	26.39	0.22	0.31	6.73
12					5	16.79	0.09	0.14	5.88
13					20	24.84	0.22	0.39	5.42
14	0.39	2.30			ft	50.84	0.25	0.24	9.74
15					10	38.15	0.15	0.11	12.62
16					15	46.19	0.21	0.16	12.57
17					30	68.79	0.37	0.23	15.46
18					5	29.17	0.08	0.00	n/a
19	0.73				20	31.03	0.27	0.32	8.19
20					30	44.96	0.39	0.36	10.40
21					10	25.46	0.20	0.18	10.95
22					35	49.91	0.43	0.47	8.82
23					5	20.20	0.08	0.07	11.23
24		4.60			15	28.86	0.22	0.31	6.98
25					10	23.60	0.16	0.21	7.36
26					5	18.65	0.07	0.15	4.56
27		1.15			20	32.89	0.28	0.27	10.01
28					30	38.77	0.39	0.28	13.58
29					40	45.88	0.49	0.28	16.81
30					10	25.77	0.14	0.16	8.76
31	1.2	2.30		20	25	44.65	0.32	0.27	11.55

32					15	37.22	0.22	0.17	12.01

Influence of cooling temperature on selectivity (ZnHy/ZnS)

No significant impact of the cooling temperature was observed on the output concentrations and selectivity. Unlike in the batch reactor, increasing the cooling water temperature has a minor impact positive effect on the kinetics of ZnHy production, which benefits selectivity.

Therefore, the temperature should be increased to improve this aspect, while limiting the temperature rise in order to maintain the SO_2 in its liquid state. In this case, the maximum temperature reached in the installation should be 67°C. This balance can later be made using the MATLAB model.

Influence of the initial zinc concentration on selectivity

The impact of the ratio H_2O/Zn is comparable to that observed in the batch reactor. An increase in the initial zinc concentration has a significant impact on the selectivity. As explained in Section 3.1, this ratio must be optimized for potential industrial applications. This improvement should be implemented carefully, to increase the zinc concentration to the level used in the industrial batch reactor, while ensuring that the system operates without the risk of clogging.

Evolution of the selectivity along the reactor

When comparing different experiments conducted under identical conditions, except for the reactor length, the evolution of the selectivity with residence time can be observed. This comparison helps assess whether extending the reactor length is advantageous regarding selectivity. In batch reactors, a decrease in pH during the reaction (due to the constant injection of SO_2) is known to be unfavorable for the production of the final product, ZnHy. However, the situation differs in the continuous reactor setup. In this system, the pH is at its lowest at the inlet, as all the SO_2 is injected at once, causing an immediate acid-base equilibrium, with no sulfur ions or H^+ ions having been consumed initially. As a result, both reactions occur at their maximum rate at the reactor entrance. As the reaction progresses along the reactor, the pH increases. However, most experiments show a decrease in selectivity as the reactor length increases. This suggests that while extending the reactor length may enhance zinc consumption, it may also reduce selectivity. Figure 9 illustrates an example of the evolution of selectivity for different reactor lengths, with all other parameters held constant.

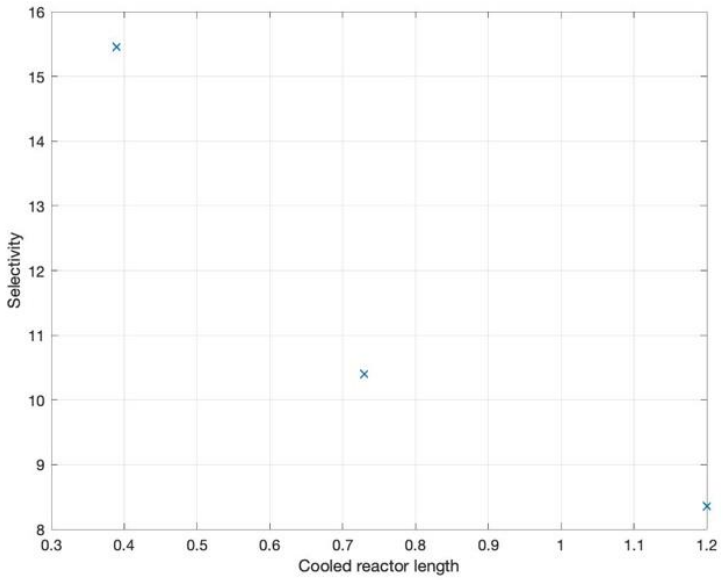

Figure 9. Evolution of the experimental selectivity as a function of the cooled reactor length (slurry flow of 210 mL/min, SO_2 flow of 30 mL/min, H_2O/Zn ratio of 2.3, cooling temperature of 5°C).

Model results

The experimental values presented in Table 2 that correspond to different input parameters (reactor length, flowrates, concentrations, temperatures) and output results were used to identify the best reaction rate laws and determine their kinetics parameters (pre-exponential factors and activation energies). The latter were computed to obtain the best fit between the reactor model results and experimental data. A nonlinear regression method was used to minimize differences between calculated and measured concentrations of zinc dithionite and zinc sulfite. During calculations, the variation range of each parameter was limited to physically sounded values (positive values for pre-exponential constants and activation energies).

The optimized parameters values from Equations 8 and 9 are as follows:

A1 = 0.736 [1/s]

Ea1 ~ 0 [J /mol]

A2 = 18615 [$m^{(0.5)}$* $mol^{(0.5)}$/s]

Ea2 = 27439 [J /mol]

The very low value of activation energy found for ZnHy production (Ea1) is consistent with Sastri's and with Kunin and Labanoy's experiments as well as with intrinsic or apparent activation energies reported for other reactions between metals and dilute aqueous acids [21], [42], [43]. The low activation energy observed could also be attributed to a limitation of the reaction rate by transport.

Figures 10A and 10B present parity plots allowing a comparison between calculated and measured values of the normalized concentrations at the outlet of the reactor. Concentrations are normalized relative to the corresponding average values at the end of the industrial process.

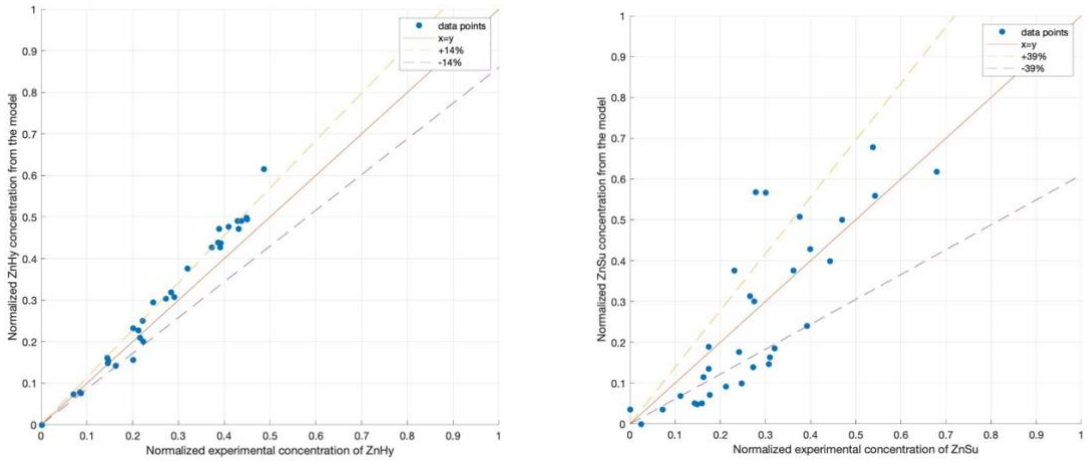

Figure 10. Comparison between normalized MATLAB model results and experimental results.

The dashed lines indicate deviations of ±14% and ±39% from the experimental concentrations of dithionite and sulfite, respectively. These intervals correspond to the mean relative errors for both species. Overall, the model aligns well with the experimental data across all cases. However, the prediction for ZnHy concentrations is more consistent compared to the results for ZnSu. This discrepancy may partially be related to the concentration ranges: as analytical errors are comparable for both compounds and since the sulfite concentration range is approximately 10 times lower than the hydrosulfite one, the relative experimental error is more significant for ZnSu. Indeed, even though the relative error for sulfite is higher, the RMSE for sulfite concentrations is 3.7 times lower that for dithionite.

The ratio between the model's RMSE and the root mean square errors of cross-validation (RMSECV) from the IR spectrometer calibration is 5.83 for zinc dithionite and 2.60 for zinc sulfite. These values indicate that the prediction errors are higher than the measurement errors, suggesting that there is still room for further refinement of the model using the available data.

Figure 11 illustrates the axial temperature profiles of the reacting medium (in blue) and of the cooling fluid (in orange). The red-shaded sections correspond to the adiabatic zones of the reactor, where there is no cooling system (static mixer zone and reactor exit). It can be observed that the evaluated temperature increase is significant in the first section (adiabatic reactor) as the kinetics are at their maximum values. Then, in the cooled section of the reactor, the temperature increases less rapidly until it reaches a maximum, after which it begins to decrease. In the final adiabatic section, the temperature increases again, but at a slower rate due to the reduced reaction rate as the reactants are almost completely consumed. The temperature of the cooling system also increases slightly, but this increase has a low impact on the conversion of the reaction and the selectivity as the reactions both have low activation energies.

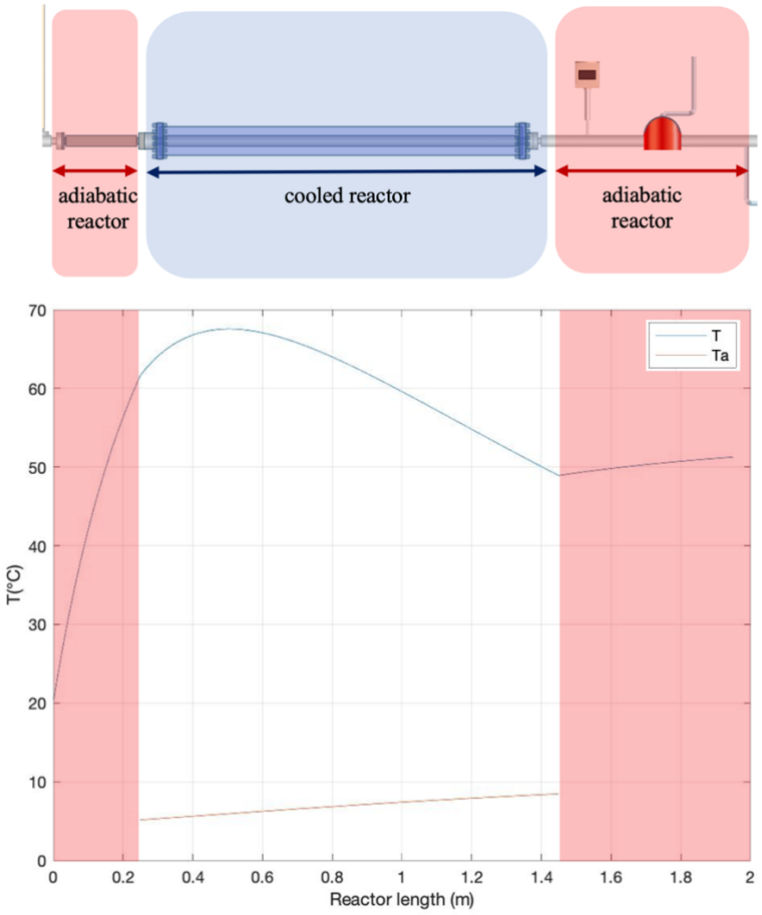

Figure 11. Example of the evaluated evolution of the reaction temperature and cooling fluid temperature along the reactor, with schematic representation of adiabatic and cooled sections. (slurry flow of 210 mL/min, SO_2 flow of 30 mL/min, H_2O/Zn ratio of 2.3, cooling temperature of 5°C).

The zinc conversion along the reactor is presented in Figure 12. Logically, the conversion increases rapidly at the beginning of the reactor, driven by the high concentration of reactants and increasing temperature, which lead to high reaction kinetics. After this initial phase, the conversion rate slows down. In the given example, zinc conversion reaches nearly 85%. The radius of the zinc particles thus decreases from 2.5 micrometers to 1.3 micrometers in this case. However, as shown in Figure 12, selectivity also decreases and tends towards a value of 10 as the reactor length increases, aligning with the experimental observations from Figure 9.

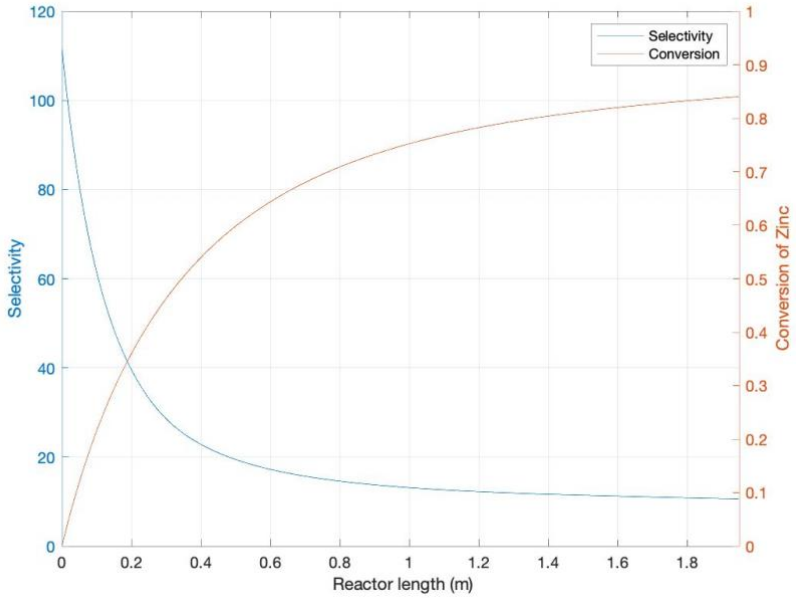

Figure 12. Example of the evaluated evolution of conversion and selectivity along the reactor. (slurry flow of 210 mL/min, SO_2 flow of 30 mL/min, H_2O/Zn ratio of 2.3, cooling temperature of 5°C)

If compared with industrial conditions, the residence time is less than 9 seconds, which is 400 times lower than in the industrial reactor. The minimum threshold for zinc conversion to meet industrial expectations is 90%. These experimental results are thus promising and indicate potential for further improvement as the reactor has not been optimized for industrial purposes yet. Also, despite the decline of selectivity, its value remains favorable and within the range of industrial expectations with a minimum threshold of 9.6. It is therefore possible to extend the reactor in order to enhance zinc conversion, allowing it to align with industrial requirements and achieve the requisite performance for industrial applications.

4. Conclusions

The utilization of a mesofluidic tubular pilot reactor shows great potential for optimizing the zinc dithionite production process. The developed pilot system demonstrated promising technical results by transitioning to a continuous operation, working under pressure to secure liquid SO_2, and using finer zinc particles to minimize clogging and fouling. Homogenization of the solid-liquid mixture was achieved using a static mixer, and product quantification was conducted in-line, transitioning from iodometric titration to infrared spectroscopy for a quicker, easier, more efficient and accurate measurement. The cooling system of the continuous setup has also proven to be effective, allowing all the SO_2 to be injected at once without exceeding the maximum temperature while maintaining selectivity above the industrial threshold value of 9.6. This design not only reduces operating time by eliminating staged SO_2 feeding but also enhances productivity by removing downtime between batches. In this study, concentrations reaching up to 49% of the maximum batch zinc hydrosulfite were obtained for a residence time of less than 9 seconds, with stable flow and no clogging.

Furthermore, the product distribution in the reactor was modeled and compared to experimental results allowing to refine the apparent kinetic parameters, thereby establishing a kinetic model crucial to optimize the future continuous industrial scale design.

One avenue for further investigations is to refine the reactor model. As Fogler noted, "*Experimentally injecting and measuring the tracer in a laminar-flow reactor can be a difficult task if not a nightmare.*" [40]. Although an ideal PFR has been assumed in this study, subsequent research could model a laminar flow reactor by solving the Navier-Stokes equations.

Modeling laminar flow with a parabolic velocity profile instead of an ideal plug flow would allow us to assess whether the actual flow pattern significantly impacts reactor performance. If no substantial effect is observed, the plug flow assumption may remain valid; however, should the influence be significant, new apparent kinetic parameters that account for the real flow conditions would need to be determined.

Another possible outlook is to investigate the reaction kinetics with different particle sizes to determine the kinetics as a function of zinc surface area. Indeed, the particle surface is included as a variable in the reaction kinetics expressions, but its actual effect on kinetics was not confirmed as a single particle size was used up to now. This approach will provide valuable insights into how the reaction kinetics are influenced by variations in zinc particle size and, consequently, the available surface area for the reaction.

Finally, to pursue industrial implementation, it will be necessary to validate upstream and downstream equipment, as well as to study the subsequent stages of the process. Nevertheless, scaling up the reactor itself should pose minimal challenges since achieving the targeted production capacity would simply involve operating the required number of reactors in parallel.

Declaration of Competing Interest

The authors declare that they have no known competing financial interests or personal relationships that could have appeared to influence the work reported in this paper.

Author's contribution statement

Jean-Luc Hoxha: Conceptualization, lab experiments, Data curation, Investigation, Software, Writing - original draft

Mathurin Grogna: Conceptualization, Formal analysis, Resources

Sébastien Calvo: Data curation, Investigation

Dominique Toye: Conceptualization, Formal analysis, Resources, Supervision, Writing - review & editing

Acknowledgements

The authors would like to express their sincere gratitude to Leen C.J. Thomassen and her team from KU Leuven for kindly providing their visualization equipment used in this study. Her support was instrumental in enabling the successful completion of this work. The authors would also like to extend their gratitude to the technical team for their invaluable support in carrying out this work.

Appendices

References

[1] V. Lakshmi Vegunta, J. S. Stevanic, M. Lindström, and L. Salmen, "Thermal and Alkali Stability of Sodium Dithionite Studied Using ATR-FTIR Spectroscopy," *Bioresources*, vol. 12, no. 2, pp. 2496–2506, Feb. 2017, doi: 10.15376/biores.12.2.2496-2506.

[2] Silox Holding, "About us - Our products and their applications." Accessed: Feb. 22, 2025. [Online]. Available: https://silox.com/about-us/

[3] J. R. Eckman and F. D. Rossini, "The Heat of Formation of Sulphur Dioxide," *J. Res. Natl. Bur. Stand.*, pp. 597–618, 1929.

[4] D. Rossini and D. Frederick, *Selected values of chemical thermodynamic properties*, U.S. Gov. Print.Off. Washington, D.C., 1952.

[5] J. D. Cox, D. D. Wagman, and V. A. Medvedev, *CODATA key values for thermodynamics*. New York: Hemisphere Pub. Corp., 1989.

[6] K. S. Elvira, X. C. i Solvas, R. C. R. Wootton, and A. J. deMello, "The past, present and potential for microfluidic reactor technology in chemical synthesis," *Nat Chem*, vol. 5, no. 11, pp. 905–915, Nov. 2013, doi: 10.1038/nchem.1753.

[7] K. Jähnisch, V. Hessel, H. Löwe, and M. Baerns, "Chemistry in Microstructured Reactors," *Angewandte Chemie International Edition*, vol. 43, no. 4, pp. 406–446, Jan. 2004, doi: 10.1002/anie.200300577.

[8] S. Ahmad, L. Ben Mustapha, S. Calvo, F. Collignon, A. E. Fernandes, and D. Toye, "Continuous flow hydrothermal synthesis of zeolite LTA in intensified reactor. Experimental and multiphysics CFD modeling approach," *Chemical Engineering and Processing - Process Intensification*, vol. 189, p. 109399, Jul. 2023, doi: 10.1016/j.cep.2023.109399.

[9] J. A. Darr, J. Zhang, N. M. Makwana, and X. Weng, "Continuous Hydrothermal Synthesis of Inorganic Nanoparticles: Applications and Future Directions," *Chem Rev*, vol. 117, no. 17, pp. 11125–11238, Sep. 2017, doi: 10.1021/acs.chemrev.6b00417.

[10] J.-C. Monbaliu and F. Collignon, "L'intensification des procédés chimiques - une approche radicale.," *Chimie et Industrie*, vol. 118, pp. 29–32, Jun. 2015, Accessed: Sep. 25, 2024. [Online]. Available: http://chimienouvelle.be/CN118web/Article%20Monbaliu.pdf

[11] S. Kuhn, K. U. Leuven, and K. Wu, "Strategies for solids handling in microreactors," 2014. [Online]. Available: https://www.researchgate.net/publication/286448225

[12] E. Dressaire and A. Sauret, "Clogging of microfluidic systems," *Soft Matter*, vol. 13, no. 1, pp. 37–48, 2017, doi: 10.1039/C6SM01879C.

[13] F. M. Akwi and P. Watts, "Continuous flow chemistry: where are we now? Recent applications, challenges and limitations," *Chemical Communications*, vol. 54, no. 99, pp. 13894–13928, 2018, doi: 10.1039/C8CC07427E.

[14] Y. Gao, B. Pinho, and L. Torrente-Murciano, "Recent progress on the manufacturing of nanoparticles in multi-phase and single-phase flow reactors," *Curr Opin Chem Eng*, vol. 29, pp. 26–33, Sep. 2020, doi: 10.1016/j.coche.2020.03.008.

[15] Z. Dong, C. Delacour, K. Mc Carogher, A. P. Udepurkar, and S. Kuhn, "Continuous Ultrasonic Reactors: Design, Mechanism and Application," *Materials*, vol. 13, no. 2, p. 344, Jan. 2020, doi: 10.3390/ma13020344.

[16] B. J. Doyle, B. Gutmann, M. Bittel, T. Hubler, A. Macchi, and D. M. Roberge, "Handling of Solids and Flow Characterization in a Baffleless Oscillatory Flow Coil Reactor," *Ind Eng Chem Res*, vol. 59, no. 9, pp. 4007–4019, Mar. 2020, doi: 10.1021/acs.iecr.9b04496.

[17] D. Fernandez Rivas and S. Kuhn, “Synergy of Microfluidics and Ultrasound,” *Top Curr Chem*, vol. 374, no. 5, p. 70, Oct. 2016, doi: 10.1007/s41061-016-0070-y.
[18] A. Vancleef, W. De Beuckeleer, T. Van Gerven, L. C. J. Thomassen, and L. Braeken, “Continuous crystallization using ultrasound assisted nucleation, cubic cooling profiles and oscillatory flow,” *Processes*, vol. 9, no. 12, Dec. 2021, doi: 10.3390/pr9122268.
[19] S. Zhao, C. Yao, Z. Dong, G. Chen, and Q. Yuan, “Role of ultrasonic oscillation in chemical processes in microreactors: A mesoscale issue,” *Particuology*, vol. 48, pp. 88–99, Feb. 2020, doi: 10.1016/j.partic.2018.08.009.
[20] P. Bianchi, J. D. Williams, and C. O. Kappe, “Oscillatory flow reactors for synthetic chemistry applications,” *J Flow Chem*, vol. 10, pp. 475–490, 2020, doi: 10.1007/s41981-020-00105-6/Published.
[21] N. V. S. Sastri, N. Epstein, A. Hirata, I. Koshijima, and M. Izumi, “Zinc hydrosulphite by three-phase fluidization: Experiments and model,” *Can J Chem Eng*, vol. 61, no. 5, pp. 635–646, Oct. 1983, doi: 10.1002/cjce.5450610504.
[22] H. L. Toor and S. H. Chiang, “Diffusion-controlled chemical reactions,” *AIChE Journal*, vol. 5, no. 3, pp. 339–344, Sep. 1959, doi: 10.1002/aic.690050317.
[23] M. Eigen, K. Kustin, and G. Maass, “Die Geschwindigkeit der Hydratation von SO2 in wassriger Losung ,” *Biol Chem*, vol. 30, pp. 130–136, 1961.
[24] M. Szabo and P. Kaldi, “A continuous method for producing ZnS2O4 solutions,” *Hungarian Journal of Industrial Chemistry* , vol. 4, pp. 39–60, 1976.
[25] S. Lynn, J. R. Straatemier, and H. Krammers, “Absorption studies in the light of the penetration theory,” *Chem. Engng. Sci.* , vol. 4, p. 49, Apr. 1955.
[26] R. A. O. Nijsing, R. H. Hendrksz, and H. Krammers, “Absorption of CO2 in jets and falling films of electrolyte solutions, with and without chemical reaction,” *Chem. Engng. Sc.*, vol. 10, pp. 88–104, 1959.
[27] N. V. S. Sastri and N. Epstein, “Chemical kinetics of zinc dissolution in sulfurous acid solutions,” *Can J Chem Eng*, vol. 56, no. 1, pp. 124–125, Feb. 1978, doi: 10.1002/cjce.5450560118.
[28] S. A. Khalil and M. A. El-Manguch, “The kinetics of zinc dissolution in nitric acid,” *Monatshefte für Chemie - Chemical Monthly*, vol. 118, no. 4, pp. 453–462, Apr. 1987, doi: 10.1007/BF00809928.
[29] O. V. Ingruber and J. Kopanidis, “Hydrosulphite bleaching part i. decomposition of hydrosulphite (dithionite) solutions with and without pulp,” *Pulp and Paper Canada*, vol. 68, no. 6, pp. 258–267, 1967.
[30] J. J. Barberá, A. Metzger, and M. Wolf, “Sulfites, Thiosulfates, and Dithionites,” in *Ullmann’s Encyclopedia of Industrial Chemistry*, Wiley, 2000. doi: 10.1002/14356007.a25_477.
[31] T. Moeller, *Inorganic Chemistry: An Advanced Textbook*, 2nd ed. New York, 1952.
[32] S. Thomas, N. Birbilis, M. S. Venkatraman, and I. S. Cole, “Corrosion of Zinc as a Function of pH,” *CORROSION*, vol. 68, no. 1, pp. 015009-1-015009–9, Jan. 2012, doi: 10.5006/1.3676630.
[33] N. Kockmann and D. M. Roberge, “Harsh reaction conditions in continuous-flow microreactors for pharmaceutical production,” Nov. 2009. doi: 10.1002/ceat.200900355.
[34] T. H. James, C. Cannon, A. Apblett, and N. F. Materer, “Sodium dithionite purity and decomposition products in solid samples spanning 50 years,” *Phosphorus Sulfur Silicon Relat Elem*, vol. 190, no. 2, pp. 158–169, 2015, doi: 10.1080/10426507.2014.914939.
[35] J. P. Danehy and C. W. Zubritsky, “Iodometric method for the determination of dithionite, bisulfite, and thiosulfate in the presence of each other and its use in

following the decomposition of aqueous solutions of sodium dithionite," *Anal Chem*, vol. 46, no. 3, pp. 391–395, Mar. 1974, doi: 10.1021/ac60339a022.
[36] TAPPI Standards Departements, "Analysis of sodium hydrosulfite - T 622 cm-10."
[37] V. Sans and L. Cronin, "Towards dial-a-molecule by integrating continuous flow, analytics and self-optimisation," Apr. 21, 2016, *Royal Society of Chemistry*. doi: 10.1039/c5cs00793c.
[38] J. L. Fox, "Sodium dithionite reduction of flavin," *FEBS Lett*, vol. 39, no. 1, pp. 53–55, Feb. 1974, doi: 10.1016/0014-5793(74)80015-3.
[39] S. Newton *et al.*, "Accelerating Spirocyclic Polyketide Synthesis using Flow Chemistry," *Angewandte Chemie International Edition*, vol. 53, no. 19, pp. 4915–4920, May 2014, doi: 10.1002/anie.201402056.
[40] S. H. Fogler, *Elements of Chemical Reaction Engineering*, 5th ed. Boston, 2016. Accessed: Feb. 21, 2025. [Online]. Available: http://search.ebscohost.com/login.aspx?direct=true&scope=site&db=nlebk&db=nlabk&AN=1601903
[41] C. Tropea, A. L. Yarin, and J. F. Foss, Eds., *Springer Handbook of Experimental Fluid Mechanics*, 1st ed. Berlin, Heidelberg: Springer Berlin Heidelberg, 2007. doi: 10.1007/978-3-540-30299-5.
[42] R. P. BELL, "The Kinetics of Reactions in Solution," *Nature*, vol. 162, no. 4112, pp. 275–276, Aug. 1948, doi: 10.1038/162275a0.
[43] T. I. Kunin and Y. A. Lobanov, "Kinetics of the Formation of Zinc Dithionite," *Izvest. Vys. Ucheb. Zaved., Khim. i Khimich. Tekh.*, pp. 921–925, 1965.